JCTC Journal of Chemical Theory and Computation

pubs.acs.org/JCTC Article

Impact of Loss Mechanisms on Linear Spectra of Excitonic and Polaritonic Aggregates

Devansh Sharma and Amartya Bose*

Cite This: https://doi.org/10.1021/acs.jctc.4c00825 Read Online

ACCESS | Metrics & More | Article Recommendations

ABSTRACT: The presence of loss mechanisms governed by empirical timescales can profoundly affect the dynamics in molecular systems, leading to changes in their spectra. However, incorporation of these effects along with the system's interaction with the thermal dissipative environments proves to be challenging. In this work, we demonstrate the possibility of utilizing the recently developed path integral Lindblad dynamics (PILD) method to study the linear spectra of molecular aggregates. PILD presents a uniquely powerful simulation technique for retaining the effects of the vibrations in a numerically exact manner through the Feynman−Vernon influence functional while incorporating the effects of losses in an empirical manner using the Lindbald master equation. As illustrations of this technique, we provide examples taken from chiral excitonic and polaritonic aggregates for which we simulate both the absorption spectra and circular dichroism (CD) spectra. We demonstrate that the effect of loss on particular states can differ not just on the basis of the symmetries of the state but also on the basis of complicated "interactions" of the structured dissipative environments with the system and its loss mechanisms. Due to the different selection rules between the absorption and CD spectra and the relative intensities and broadening of the peaks, the two linear spectra together give an interesting insight into the contributions of the various eigenstates to the correlation functions. While the focus here is on linear spectroscopy, it should be possible in the future to use PILD to study multidimensional spectra under loss mechanisms as well.

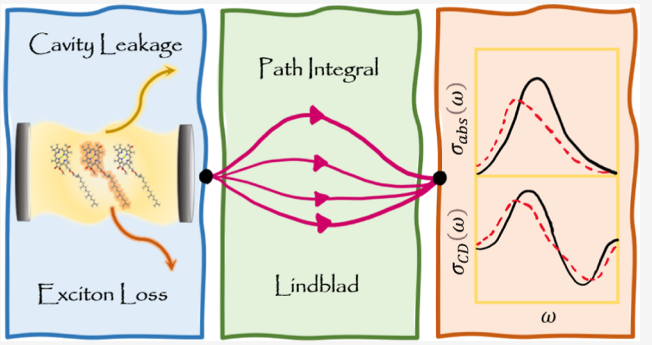

1. INTRODUCTION

Spectroscopy is one of the most basic tools for characterizing chemical systems. While absorption spectra give an insight into the electronic structure, circular dichroism (CD) spectra provide insights into the geometry of chiral systems. These spectra are broadened due to the coupling of the eigenstates to environment degrees of freedom, which are usually thermally populated. Simulations of the exact line shape proves to be challenging owing to the continuous manifold of environmental states participating in the dynamics. The presence of loss mechanisms in many systems additionally broadens the spectral features in probably unpredictable ways. This extra broadening due to loss mechanisms poses a further challenge to any predictive endeavor. Methods based on wave functions such as density matrix renormalization group[1−4] or multiconfiguration time-dependent Hartree[5] and its multilayer formulation[6,7] have been pushing the limits of what is computationally tractable; however, they still are inadequate in describing the dynamics in the condensed phase where a continuum of environment degrees of freedom are thermally populated.

Methods that simulate the reduced density matrix (RDM) of the system overcome many of these challenges by integrating an appropriately selected set of environment modes. This tracing over the environment, however, makes the dynamics non-Markovian. Various approximate methods like the Bloch−Redfield master equation[8,9] and the Lindblad or the Gorini−Kossakowski−Sudarshan−Lindblad master equation[10,11] treat the bath perturbatively or make a Markovian approximation for the dynamics. Generally for strongly coupled condensed phase environments, such perturbative methods perform poorly. Mixed quantum classical methods like surface hopping[12,13] treat the environment classically and make ad hoc approximations about the nonadiabatic transitions. The biggest problem with these methods is that while simple, their results cannot be improved systematically. Feynman's path integral approach[14] provides an alternate route to simulating such systems that is numerically rigorous. The environment modes

Received: June 25, 2024
Revised: September 4, 2024
Accepted: October 1, 2024

are incorporated in a nonperturbative manner using the Feynman−Vernon influence functional.[15] The hierarchical equation of motion[16,17] and the quasi-adiabatic propagator path integral (QuAPI)[18,19] and later developments on them[20−29] provide lucrative ways of implementing path integral for large open quantum systems. Recent applications on large biomolecular aggregates[29−32] show the full power and applicability of these methods in simulating large systems.

While exact quantum dynamical simulations are becoming increasingly feasible through the combination of path integral methods and tensor network methods,[26,33] these methods demand detailed characterization of the system−environment interaction through the spectral density. This can often be quite challenging. Consider, for example, the loss of an exciton at particular sink sites to the "special pair" in photosynthetic aggregates, the spontaneous emission of the excited state of molecules in a Frenkel exciton transport chain, or the loss of photons from leaky cavities. While in principle, one can describe these processes using harmonic environments, it is not always possible to characterize such environments using proper spectral densities. The commonly used Gardiner−Collett form,[34] for instance, describes a leaky cavity using a flat bath spectrum where the system−environment coupling constant is independent of the frequency. Use of such fictitious baths can often induce artifacts stemming from the particular functional form used, which is not uniquely defined.[35] In addition to these spectral density-related artifacts, one also increases the cost of the simulation. For most of these loss processes, the relevant timescale is probably the single most reliable property that is available. Further information about the form of the spectral density often stems from assumptions of convenience about the system. In such cases, it can often be more judicious to forego an attempt to describe the environment and resort to incorporation of the effect solely through the empirical timescale that is readily available.

Dissipative dynamics governed by empirical timescales can be described quite efficiently by non-Hermitian descriptions of the system. However, the non-Hermiticity results in non-unitary dynamics, which leads to spurious effects in correlation functions and spectra. The Lindblad master equation, which maintains the unitarity of evolution, offers a lucrative alternative to these non-Hermitian descriptions in simulating such systems. Now, while the Lindblad approach is good for the loss mechanisms, it is not accurate for incorporating the non-Markovian effects of thermal vibrations. A combination of the fully semiclassical partial linearized density matrix[36,37] with the Lindblad master equation has been used to study the effect of losses on the 2D electronic spectra of polaritonic aggregates by Mondal et al.[38]

Recently, one of us has developed an efficient approach toward combining numerically exact QuAPI simulations, accounting for the nonperturbative non-Markovian bath effects, with the Lindblad master equation to account for such empirical loss mechanisms at no extra cost.[39] This path integral Lindblad dynamics (PILD) approach guarantees a positive definite dynamical map for the dynamics. Being based on QuAPI, it is able to handle arbitrary structured thermal environments fully quantum mechanically. Moreover, different loss mechanisms can be studied at no additional cost. The impact of the loss of an exciton on the dynamics in the Fenna−Matthews−Olson complex was explored.[39]

Here, we extend the PILD approach to simulate the line-shapes of linear spectra of aggregates in the presence of loss and attempt to answer the natural question: how does the spectrum of a system get affected by the presence of these loss mechanisms? Can we quantitatively simulate the spectra in the presence of these losses without losing accuracy in terms of describing the thermal vibrations in the system? These losses become especially interesting in cases of excitonic molecular wires where the exciton is lost at one site and excitonic polaritons where the cavity is known to be lossy. In Section 2, we summarize the PILD framework[39] and extend it to allow the study of linear spectra. In Section 3, we describe the chiral molecular aggregates that are of interest. We explore the absorption and CD spectra under different loss cases, incorporating the full effects of the structured thermal environment. While one might be tempted to make simple generalizations about the impact of loss on the absorption and CD spectra, it seems that little can be simply stated beyond the fact that loss, in general, broadens peaks and decreases their intensities. We show that which peak is broadened and by what amount is a nontrivial problem. While we try to find rules of thumb that provide more insight, the complex nature of the emergent phenomena makes it practically impossible to do so. Consequently, it is important to have a way to simulate a system rigorously and to discover the effects in a particular case. It is this exercise that is enabled by PILD, which allows for a simple incorporation of processes described by empirical timescales in rigorous numerical simulations for the first time. Finally, we end by providing some concluding remarks and future directions in Section 4.

2. METHOD

Consider an open quantum system described by a system−environment decomposed Hamiltonian

$$H = H_0 + H_{\mathrm{env}} \tag{1}$$

where H_0 is the system Hamiltonian and H_{env} is the Hamiltonian describing the environment and its interaction with the system. For a typical exciton transport system, the system can be defined in terms of the singly excited subspace spanned by $|j\rangle$ representing the excitation occurring on the jth molecule, with all other molecules in the ground state. The resultant Hamiltonian has the well-known Frenkel form

$$H_0 = \sum_{j>0} \varepsilon_j |j\rangle\langle j| + \sum_{j>k>0} h_{jk}(|j\rangle\langle k| + |k\rangle\langle j|) \tag{2}$$

where ε_j is the energy of the locally excited state on the jth molecule and h_{jk} is the amplitude for the excitation to hop from the jth to the kth molecule. Notice that this Hamiltonian is expressed in the so-called first-excitation subspace. For the simulation of spectra, it will be necessary to augment the basis with the electronic ground state, $|0\rangle$, which has all of the monomers in the ground state.

The environment includes the thermal solvent to which the system is exposed and the molecular vibrations of the system. Under linear response, these modulations can be mapped on to baths of harmonic oscillators that locally interact with a monomer

$$H_{\mathrm{env}} = \sum_{j>0} \sum_{b} \frac{p_{jb}^2}{2} + \frac{1}{2}\omega_{jb}^2 x_{jb}^2 - c_{jb} x_{jb} |j\rangle\langle j| \tag{3}$$

where ω_{jb} is the frequency of the bth harmonic mode that interacts with the jth molecule and c_{jb} is the corresponding

https://doi.org/10.1021/acs.jctc.4c00825
J. Chem. Theory Comput. XXXX, XXX, XXX−XXX

coupling. The mapping of a molecular solvent onto this set of harmonic baths is done through the bath spectral density

$$J_j(\omega) = \frac{\pi}{2}\sum_b \frac{c_{jb}^2}{\omega_{jb}}\delta(\omega - \omega_{jb}) \tag{4}$$

For a molecular solvent, $J_j(\omega)$ can be calculated using molecular dynamics simulations.[40−42] In addition to this environment, the system also has loss mechanisms that cannot be readily described in this Hamiltonian formalism. These would be incorporated using the Lindblad master equation[10,11] using a set of Lindbladian jump operators, L_j. Therefore, we need a way to simulate the RDM of the system in the presence of both the thermal environment and the jump operators.

According to the PILD[39] approach, the loss mechanisms are incorporated using a modified Nakajima−Zwanzig master equation.[43,44] If the initial state is uncorrelated, $\rho(0) = \tilde{\rho}(0) \otimes \exp(-\beta H_{env})/Z$, then the time-evolution of the RDM corresponding to the system is given by[39]

$$\dot{\tilde{\rho}}^{(L)}(t) = -\frac{i}{\hbar}\mathcal{L}_0\tilde{\rho}^{(L)}(t) + \int_0^{\tau_{mem}} \mathcal{K}(\tau)\tilde{\rho}^{(L)}(t-\tau)\,d\tau + \sum_j \left(L_j\tilde{\rho}^{(L)}(t)L_j^\dagger - \frac{1}{2}\{L_j^\dagger L_j, \tilde{\rho}^{(L)}(t)\}\right) \tag{5}$$

where $\tilde{\rho}^{(L)}(t)$ is the time-evolved RDM for the open quantum system under the influence of the Lindbladian jump operators, $\mathcal{L}_0 = [H_0, \cdot]$ is the system Liouvillian, $\mathcal{K}$ is the memory kernel corresponding to the thermal environment, and τ_{mem} is the memory length.

Obtaining the memory kernel, $\mathcal{K}$, is extremely challenging because of a circular dependence of $\mathcal{K}$ on the dynamics of the reduced system. Various approaches have evaluated $\mathcal{K}$ using the dynamics from uncontrolled approximations like classical trajectory simulations.[45,46] Previous work[46] has shown that using these approximate memory kernels to solve the Nakajima−Zwanzig master equation leads to dynamics that is significantly more accurate than the dynamics that produced the memory kernel. We, on the other hand, use the framework of transfer tensor method,[20] which decomposes the dynamical maps, $\mathcal{E}(t)$, of the reduced system defined by $\tilde{\rho}(t) = \mathcal{E}(t)\tilde{\rho}(0)$, in terms of transfer tensors T_k defined as

$$T_k = \mathcal{E}(k\Delta t) - \sum_{k>m\geq 1} T_m\mathcal{E}((k-m)\Delta t) \tag{6}$$

such that the time evolution of the system can be expressed as

$$\tilde{\rho}(t_n) = \sum_{k=1}^{L} T_k\tilde{\rho}(t_{n-k}) \tag{7}$$

where $L\Delta t = \tau_{mem}$. These transfer tensors can now be related to the memory kernel as

$$T_k = \mathcal{E}_0(\Delta t)\delta_{k,1} + \mathcal{K}_k\Delta t^2 \tag{8}$$

where $\mathcal{E}_0(t) = \exp(-iH_0t/\hbar) \otimes \exp(iH_0t/\hbar)$ is the dynamical map corresponding to the bare system, H_0.

To obtain the transfer tensors T_k, and consequently the memory kernels $\mathcal{K}_k$, the dynamical maps, $\mathcal{E}(t)$, are simulated using path integrals. These dynamical maps propagate the RDM of the system in the presence of the environment. Suppose that at the initial time, the system is in a separable state with the environment in a thermal equilibrium, $\rho(0) = \tilde{\rho}(0) \otimes \exp(-\beta H_{env})/Z$. Then the dynamical map of the system in the presence of the environment can be obtained using nonperturbative, numerically exact path integral methods[18,19]

$$\tilde{\rho}(N\Delta t) = \mathcal{E}(N\Delta t)\tilde{\rho}(0) \tag{9}$$

$$\langle s_N^\pm|\mathcal{E}(N\Delta t)|s_0^\pm\rangle = \sum_{s_1^\pm}\cdots\sum_{s_{N-1}^\pm}\langle s_N^\pm|\mathcal{E}_0(\Delta t)|s_{N-1}^\pm\rangle \times \langle s_{N-1}^\pm|\mathcal{E}_0(\Delta t)|s_{N-2}^\pm\rangle\cdots \times \langle s_1^\pm|\mathcal{E}_0(\Delta t)|s_0^\pm\rangle F[\{s_i^\pm\}] \tag{10}$$

where $s_i^\pm$ is the state of the system at ith time point and $F[\{s_i^\pm\}]$ is the Feynman−Vernon influence functional[15] along the path $\{s_i^\pm\}$, which makes the dynamics non-Markovian. The interactions between different time points caused by environmental effects, which are encoded in the influence functional, are related to the spectral density, eq 4, and the bath response function.[42] Once the bath has been properly parameterized, there are no further approximations involved in eq 10.

With the memory kernels $\mathcal{K}_k$ in hand, we discretize eq 5 to finally get the RDM at the nth time-step with the incorporation of loss mechanisms[39]

$$\tilde{\rho}_n^{(L)} = \mathcal{E}_0(\Delta t)\tilde{\rho}_{n-1}^{(L)} + \sum_{k=1}^{L}\mathcal{K}_k\tilde{\rho}_{n-k}^{(L)}\Delta t^2 + \sum_j\left(L_j\tilde{\rho}_{n-1}^{(L)}L_j^\dagger - \frac{1}{2}\{L_j^\dagger L_j, \tilde{\rho}_{n-1}^{(L)}\}\right)\Delta t \tag{11}$$

Equation 11 encodes the nonequilibrium dynamics of the reduced density matrix of the system. The goal here is to simulate the line shape of the linear spectra of the system. To this end, an arbitrary linear spectra is related to the Fourier transform of a system time correlation function of the form

$$C_{A-B}(t) = \mathrm{Tr}[A(t)B(0)\rho(0)] \tag{12}$$

where $\rho(0)$ is the initial equilibrium density matrix, and A and B are the appropriate system operators. While simulation of time-correlation functions using the Nakajima−Zwanzig master equation formalism typically requires one to account for the initial correlation between the system and the bath through an additional correction term, it is generally not possible to give a closed-form representation to this term. However, one can "learn" it from exact simulations.[47] Interestingly, given the structure of the Frenkel−Holstein Hamiltonian and that of the absorption and CD spectra, the initial equilibrium density matrix can often be replaced by a density matrix with no initial system environment correlation

$$\rho(0) = \tilde{\rho}(0) \otimes \frac{\exp(-\beta H_{env})}{Z_{env}} \tag{13}$$

which obviates the need for the correction term in the master equation. (Notice that this is not always the case. For instance, in the case of simulating the emission spectrum, one cannot construct an uncorrelated initial condition. One has to necessarily take care of the simultaneous system−environment

https://doi.org/10.1021/acs.jctc.4c00825
J. Chem. Theory Comput. XXXX, XXX, XXX−XXX

equilibration. However, for absorption and CD spectra, this is true.) One can define a time-evolved quantity

$$\rho_B(t) = \mathrm{Tr}_{\mathrm{env}}[\exp(-iHt/\hbar)B\rho(0)\exp(iHt/\hbar)] \tag{14}$$

which can be computed using PILD for an arbitrary environment. Now, the correlation function can be obtained as $C_{A-B}(t) = \mathrm{Tr}_{\mathrm{sys}}[A\rho_B(t)]$. The subscripts, sys and env, denote partial trace over system and environment degrees of freedom, respectively.

The two specific cases of linear spectra that are studied here as examples are the absorption and CD spectra. The absorption spectra is the real part of the Fourier transform of the transition dipole moment autocorrelation function[48] ($A = B = \mathrm{f}\mu$)

$$\sigma_{\mathrm{abs}}(\omega) \propto \mathrm{Re}\left[\int_0^\infty e^{i\omega t} C_{\mu-\mu}(t)\, \mathrm{d}t\right] \tag{15}$$

where $\mu = \sum_j \mu_j$ is the total transition dipole moment constituted by the individual molecular transition dipoles, μ_j. For a molecular aggregate, the CD spectrum is defined in terms of the correlation function with $A = m$ and $B = \mu$ as[48]

$$\sigma_{\mathrm{CD}}(\omega) \propto \mathrm{Im}\left[\int_0^\infty e^{i\omega t} C_{\mu-m}(t)\, \mathrm{d}t\right] \tag{16}$$

where the magnetic moment of the aggregate, $m = \frac{i}{2\hbar}\sum_j \varepsilon_j(\vec{r}_j \times \mu_j)$ given that the jth molecule with a transition dipole of μ_j and excitation energy ε_j is located at $\vec{r}_j$. The CD spectrum is instrumental in analyzing orientational chirality in molecular aggregates. Using the correlation function-based definitions of the spectra allows for an exact simulation of the line shape for a particular environment at a particular temperature.

3. NUMERICAL RESULTS AND ANALYSIS

As illustrations of simulating spectra using PILD, we explore the spectra of two different classes of systems, the first being that of an excitonic molecular aggregate, which is described by a Frenkel–Holstein Hamiltonian given in eq 1. The corresponding system as defined by eq 2 has N bacteriochlorophyll (BChl) molecules of equal monomer excitation energy ($\varepsilon_j = \varepsilon$ for all j) that interact in a nearest-neighbor fashion ($h_{j,k} = 0$ for $|j-k| > 1$) in two different geometries, the right-handed helix ($h_{j,j+1} = 363\ \mathrm{cm}^{-1}$) and the right-handed creeper ($h_{j,j+1} = -363\ \mathrm{cm}^{-1}$) where the coupling strength $h_{j,j+1}$ reported by Tretiak et al.[49] has been used. Notice that the helix is an H-aggregate, whereas the creeper is a J-aggregate. The consecutive individual molecular transition dipoles of both arrangements are rotated counterclockwise by $\frac{\pi}{6}$. For the helix, the molecular centers are all aligned along the z-axis, whereas the displacement vectors for consecutive molecules make an angle of $\frac{\pi}{4}$ with the z-axis and the projections of their position vectors in the xy-plane make an angle of $\frac{\pi}{6}$ with each other for the creeper geometry. The intermolecular distance for the creeper is 0.79 times that of the helix. Both of these arrangements are graphically depicted in Figure 1. We will refer to these nonplanar aggregates with nonparallel transition dipole moments simply as nonplanar aggregates, while any planar aggregate with parallel transition dipole moments will be called a planar aggregate.

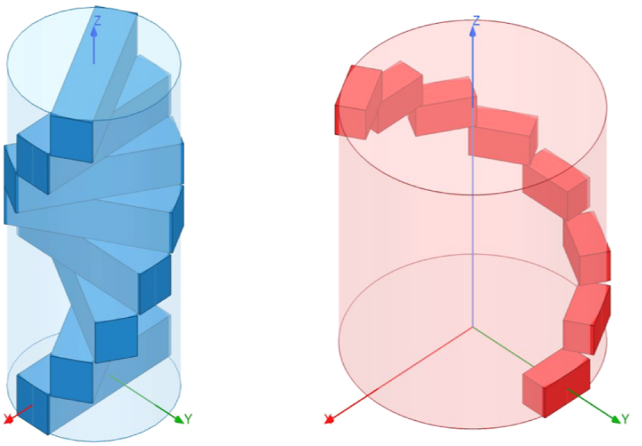

Figure 1. Geometries of molecular aggregates: right-handed helix (left, blue) and right-handed creeper (right, red).

The vibrations associated with the BChl monomers have been incorporated using the Huang–Rhys factors corresponding to the 50 most strongly coupled vibrations as reported by Rätsep et al.[50] These include only relatively rigid molecular vibrations which contribute sharp features to the spectral density. To make the system more realistic, we have augmented the spectral density using a Brownian bath described by a Drude–Lorentz spectral density with a reorganization energy of 109 cm^{-1} and broadened the aforementioned sharp features stemming from the rigid vibrations using Lorentzians of width 10.97 cm^{-1}. The resultant spectral density is shown in Figure 2. The

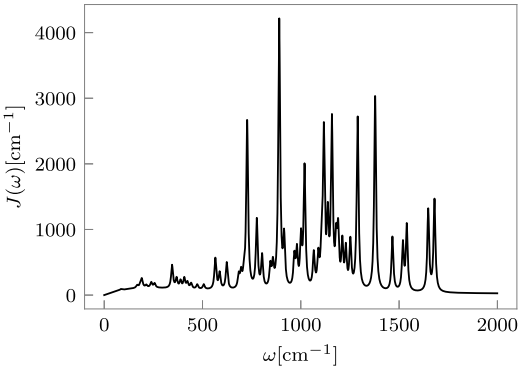

Figure 2. Spectral density corresponding to a BChl molecule with a total reorganization energy of 327 cm^{-1}.

temperature is set to 300 K. The dynamics of systems with such structured and strongly coupled environments is particularly difficult to simulate for many approximate methods.

The second class of systems whose spectra we explore is excitonic–polaritonic in nature. The same BChl aggregates that were described below are put inside a cavity. The system can now be written as

$$H_0 = \sum_j \varepsilon_j |j\rangle\langle j| + \sum_j h_{j,j+1}(|j\rangle\langle j+1| + |j+1\rangle\langle j|) + \hbar\omega_c |c\rangle\langle c| + \frac{1}{\sqrt{N}}\sum_j \Omega_j(|c\rangle\langle j| + |j\rangle\langle c|) \tag{17}$$

https://doi.org/10.1021/acs.jctc.4c00825
J. Chem. Theory Comput. XXXX, XXX, XXX–XXX

where $|c\rangle$ is the state with all the molecules in the ground state and the cavity in the excited state, ω_c is the frequency of the cavity, and Ω_j is the coupling of the jth monomer to the cavity. Assuming the electric field of the cavity mode to be aligned with transition dipole moment of the first monomer, we take $\Omega_j = \Omega\cos\left((j-1)\frac{\pi}{6}\right)$ where $\Omega = 403.28\ \text{cm}^{-1}$ and $\hbar\omega_c = \varepsilon$, which is the common excitation energy for all the monomers. It is also important to note that the cavity is not coupled to a thermal environment.

Both spectra are governed by correlation functions involving the total transition dipole moment of the aggregate. This is obtained as

$$\mu = \sum_j \vec{\mu}_j(|j\rangle\langle 0| + |0\rangle\langle j|) \tag{18}$$

Notice that the transition dipole moment operator does not involve the cavity.

We will explore the effect of loss from a particular monomer, $|j\rangle$, with a decay time constant, τ, on the absorption and CD spectra in various cases. This can be described by the Lindblad operator $L_j = \tau^{-1/2}|0\rangle\langle j|$. Additionally, in the cases of excitonic-polaritons, the cavities are generally leaky. This loss can be captured by the corresponding Lindblad operator $L_c = \tau_c^{-1/2}|0\rangle\langle c|$. The simulations are done using the path integral Lindblad method[39] with the transfer tensors being generated using the time-evolving matrix product operator algorithm[23] with multiple baths[33] as implemented in the open-source QuantumDynamics.jl simulation framework.[51] The inclusion of loss through PILD guarantees certain conserved quantities in the form of sum rules. The area under the linear spectra, being related to the zero time value of correlation functions, is invariant with the loss incorporated in the system.

3.1. Spectroscopy of Excitonic Molecular Aggregates.

We start by exploring the spectra of the excitonic molecular aggregates under losses with different decay times. Consider a BChl dimer in the creeper and the helix formations. In Figure 3, we show the absorption and CD spectra for the system with decay times τ = 25, 50, and 75 fs along with that of the loss-less dimer (in solid curve). The profile of the absorption peak of helix is significantly more structured and broader than that of the creeper. It is usual for H-aggregates to have more broadened spectra compared to the J-aggregates when coupled with structured vibrational bath among other factors.[52]

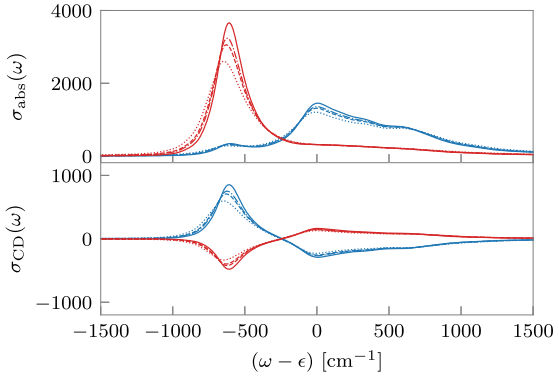

Figure 3. Absorption and CD spectra of BChl dimers in helix (blue) and creeper (red) geometries for different decay times, τ = 25 (dotted), 50 (dashed), and 75 fs (dash-dot) and the loss-less case (solid).

However, unlike the usual planar H- and J-aggregates, these chiral dimers do not necessarily have only a single peak. Both of the eigenstates can be bright, as seen quite clearly in the helix absorption spectrum. The CD spectrum shows a positive first and a negative second Cotton feature for the helix geometry, which is opposite to that of the creeper geometry despite both geometries being right-handed.

It is notable that, while the two expected peaks corresponding to the two bright excitonic states for a nonplanar dimer are not easily discernible from the absorption spectrum (especially for the creeper), it is possible to clearly locate them from the CD spectrum due to the switching signs and all over lower absolute amplitude of the latter. The absorption spectrum is positive semidefinite. Consequently, the broad intense peaks can more easily overshadow the nearby peaks. Furthermore, the relative intensities of the absorption spectrum and the CD spectrum are also different because of the different correlation function they derive from. For the absorption spectrum, even in absence of the vibrations, there would be a differential intensity for the two different peaks corresponding to the two eigenstates (see Table 1 in Appendix C). The extreme case is that of the planar J- and H-aggregates, which completely suppress the peak intensity for the lower and the higher excitonic peak, respectively. In CD spectra, this is not the case. As we demonstrate in Appendix C, the intensities for both peaks have the same relative magnitude in the absence of the vibrational environment. Thus, the difference in intensity that we see between the two peaks of the CD spectrum in Figure 3 is an effect of the environment alone.

In Figure 3, it is clearly seen that although both the helix and the creeper geometries have the same absolute chirality, the CD spectra have different Cotton effects. This is in apparent contradiction of the often-used exciton-chirality (EC) rule, which uniquely maps the sign of the lowest-energy Cotton couplet to the absolute chirality of the aggregate.[53−55] However, Swathi et al.[56] have shown that, consistent with our results here, the EC mapping is reversed between the H- and J-dimers. Finally, it should be mentioned that there is no reason to expect the broadening of the peaks in the absorption spectrum and the CD spectrum to be similar.

With stronger losses, we note in Figure 3 that the attenuation of the spectral features increases, and there is a corresponding broadening of the peaks in order to satisfy the previously mentioned sum rule that keeps the area under a linear spectrum constant. This is also accompanied by an increasing red shift of the absorption spectrum. (This is also seen in the absence of the dissipative environment as demonstrated in Appendix A.) The red shift of the $\omega < \varepsilon$ peak seems to be higher than that of the $\omega \geq \varepsilon$ peak. These observations also extend to the CD spectrum, where the shift and attenuation due to loss mechanisms are apparently more prominent for the sharper peaks (or troughs).

From the dimer as a representative case, we proceed to investigate the effect of exciton system size vis-à-vis decay time τ in Figure 4a,b. We look at the dimer, trimer, tetramer, and pentamer with the same nearest-neighbor intermolecular couplings. Losses with a decay time of τ = 50 fs are applied to each of the unique sites in the aggregate. For the trimer and tetramer, monomers 1 and 2 constitute the two distinct sites of decay, while for the pentamer, monomer 3 is an additional unique site. While we observe a red shift in the absorption spectra for the J-creepers, where all peaks lie in the region $(\omega - \varepsilon) < 0$ (Figure 4b), there is a blue shift for the H-helices for

https://doi.org/10.1021/acs.jctc.4c00825
J. Chem. Theory Comput. XXXX, XXX, XXX−XXX

Table 1. Absorption and CD Peak Heights for Isolated Excitonic Aggregates as a Function of Aggregate Size[a]

excitonic aggregate	helix			creeper		
	ω' (cm^{-1})	$\sigma_{CD}(\omega')$	$\sigma_{abs}(\omega')$	ω' (cm^{-1})	$\sigma_{CD}(\omega')$	$\sigma_{abs}(\omega')$
dimer	−363.0	+0.5	0.13	−363.0	−0.5	1.86
	+363.0	−0.5	1.86	+363.0	+0.5	0.13
trimer	−513.86	−0.16	0.02	−513.36	−1.57	2.45
	0.0	+1.73	0.50	0.0	+1.73	0.50
	+513.36	−1.57	2.45	+513.36	−0.16	0.02
tetramer	−587.35	+0.09	0.04	−587.35	−3.19	2.81
	−224.35	−0.31	0.02	−224.35	+3.41	1.06
	+224.35	+3.41	1.06	+224.35	−0.31	0.02
	+587.35	−3.19	2.81	+587.35	+0.09	0.04
pentamer	−628.73	0.0	0.0	−628.73	−5.20	2.99
	−363.0	+0.10	0.13	−363.0	+5.10	1.86
	0.0	0.0	0.0	0.0	0.0	0.0
	+363.0	+5.10	1.86	+363.0	+0.10	0.13
	+628.730	−5.20	2.99	+628.73	0.0	0.0

[a] $\omega' = \omega - \varepsilon$.

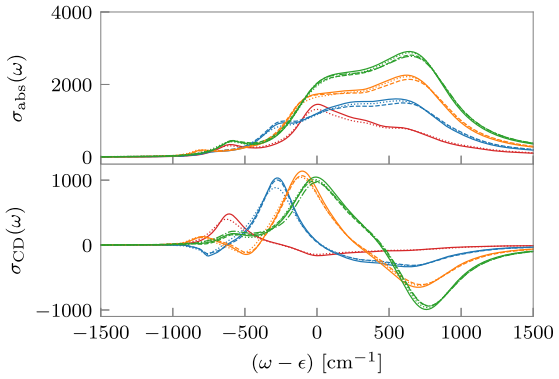

(a) Helix geometry

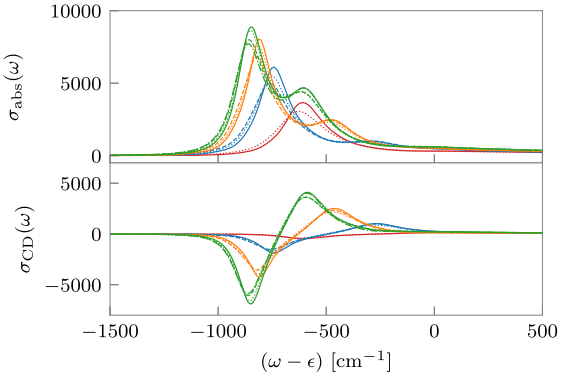

(b) Creeper geometry

Figure 4. Absorption and CD spectra of BChl dimer (red), trimer (blue), tetramer (orange), and pentamer (green) for decay time of τ = 50 fs at monomer 1 (dotted), monomer 2 (dashed), monomer 3 (dash-dot), and the loss-less cases (solid).

peaks in the region $(\omega - \varepsilon) \geq 0$ and a red shift for peaks in the complementary region for all system sizes on the inclusion of loss (Figure 4a). This is a consequence of the presence of the thermal environment. (Absence of the thermal bath leads to the peaks coming closer to each other and to ε, as we discuss further in Appendix A.) The impact of a loss on a single site is seen to decrease with increasing system size. Moreover, decay at the central monomer is more effective in attenuating the intensity of spectrum than the decay at other sites owing to symmetries of the system.

For the J-type creepers, the sign of the first CD peak is consistently seen to be negative at all sizes of the aggregates. However, it is interesting that all of the H-type helices do not show the same sign of the first peak of the CD spectra. For the case of the helix trimer, one sees the initial peak become negative instead of the positive peak seen in the other helices. This further shows that the EC mapping between the CD spectra and the corresponding geometry is more tenuous. Earlier, we discussed the inconsistency between a helix and creeper dimer. Now we note the inconsistency between helices of different sizes. However, this pattern can be explained for the bare system through a calculation of the rotational strengths[48,57] of each of the excitonic states as outlined in Appendix B. Also, as seen in the case of the isolated pentamer (Table 1 in Appendix C), for both the creeper and the helix, there are only three states that are CD active.

3.2. Spectroscopy of Excitonic−Polaritonic Systems.

As a second class of systems of interest, we consider excitonic systems coupled with a plane-polarized cavity mode. In Figure 5, we see how upon coupling to the cavity mode, a monomer absorption peak splits into two polaritonic peaks correspond-

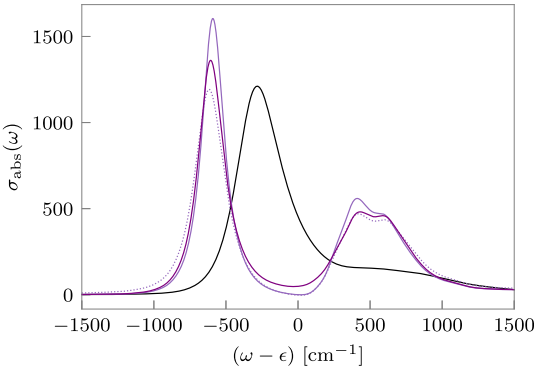

Figure 5. Absorption spectrum of BChl monomer with (purple) and without (black) an optical cavity for decay time of τ = 50 fs at monomer (dotted), cavity (solid; darker shade), and the loss-less case (solid; lighter shade).

https://doi.org/10.1021/acs.jctc.4c00825
J. Chem. Theory Comput. XXXX, XXX, XXX−XXX

ing to the lower energy "lower polariton" and higher energy "upper polariton", which are the two eigenstates of eq 17. In the absence of any loss, the upper polariton shows a broader line shape, which correlates with a shorter lifetime in comparison to the lower polariton. We notice that, similar to the excitonic systems, the decrease in intensity and broadening of peaks on the inclusion of loss mechanisms are not equal. It is more for the lower polariton than for the upper polariton.

The difference between the impact of the cavity loss and the monomer loss becomes especially noticeable for the lower polariton. This is entirely due to interaction of the environment with the different polaritons because the contributions of the monomer and the cavity to both the polaritons are half. Consequently, if the only effect was how much was the leaky site contributing to the polariton, both peaks should behave identically. Here, we notice that the lower polariton $|L\rangle$ experiences a red shift, while the upper polariton $|U\rangle$ experiences a blue shift, leading to an increase in the Rabi splitting (the energy difference between $|L\rangle$ and $|U\rangle$). This emergent phenomenon corresponds to the strong coupling regime as discussed using the $P(E)$ theory.[58,59] However, while the $P(E)$ theory deals with the environment in an approximate manner, using PILD, we quantitatively account for the effects of the thermal environment in a nonperturbative manner through the Feynman–Vernon influence functional.[15] This effective expansion of the polaritonic spectrum is opposite to the compression observed in the absence of the dissipative environment, as demonstrated in Appendix A, and consequently enabled by the presence of the dissipative environment.

Finally, in Figure 6a,b, we demonstrate the absorption and CD spectra for the BChl dimer and trimer coupled to a cavity mode. While a polaritonic system described by the popular Holstein–Tavis–Cummings (HTC) model has only two bright states,[60] here we have more. The appearance of only two bright states in the absorption spectrum of the HTC model is a result of the model dealing with planar aggregates with no intermonomer couplings. In fact, a violation of either of these two conditions can increase the number of bright states. We demonstrate this in Appendix C where we list the intensities of the CD and absorption peaks corresponding to the different polaritons. Additionally, while we see an exact reversal of peak positions and their absorption and CD intensities for an isolated system between the helix and creeper as noted in Table 2 of Appendix C, the thermal environment disrupts this, otherwise, symmetric change.

We further notice in both geometries that the effect of a loss at the cavity is qualitatively different from that at the monomers, which, of course, is expected since, unlike the monomers, the cavity is not coupled to a thermal environment. Moreover, none of the monomeric sites are equivalent due to different monomer-cavity couplings Ω_j, and consequently, the impact of loss at each monomer is different which, in particular, is more pronounced for the case of the trimer where $\Delta\Omega_{j,k}(=|\Omega_j - \Omega_k|)$ is larger than that for the dimer. For the helix geometry, the lowest and highest energy CD peaks seem to remain relatively unaffected by cavity loss. The intermediate peaks are all highly damped. The effect seems to be reversed for the creeper geometry (Figure 6b). This is again due to the differential impact of the thermal environment on peaks lying on either side of $\omega = \varepsilon$. Thus, there is a more marked decrease in the lifetime of particular polaritons due to the loss mechanisms in the presence of thermal environment.

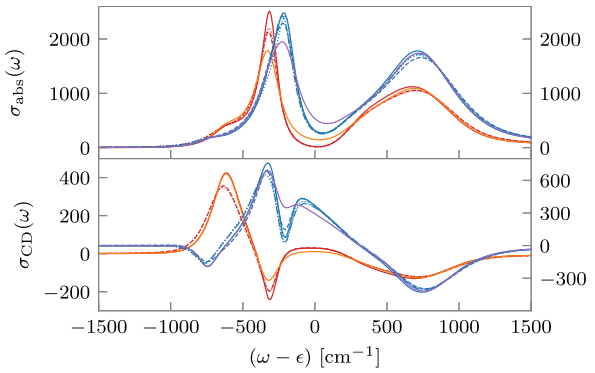

(a) Helix geometry

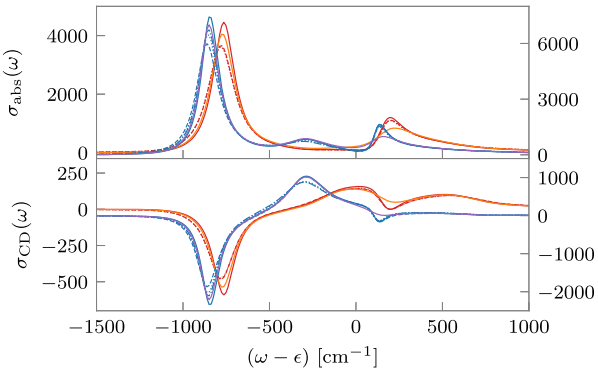

(b) Creeper geometry

Figure 6. Absorption and CD spectra of BChl dimer (red; left y-axis) and trimer (blue; right y-axis) in an optical cavity for decay time of τ = 50 fs at monomer 1 (dotted), monomer 2 (dashed), monomer 3 (dash-dot), cavity (dimer: orange, trimer: purple), and the loss-less cases (solid).

Additionally, it is interesting that the first CD couplet resembles the excitonic system, but one must be cautious in inferring the geometry of the aggregate solely from the first CD couplet as the broadening and attenuation of two close peaks due to the thermal environment may lead to misleading signs of CD peaks as in the case of the creeper dimer where the second CD peak is positive despite the isolated creeper dimer having a negative intensity for the same (see Table 2 in Appendix C).

4. CONCLUSIONS

In this paper, we present a numerically rigorous study of the impact of empirically described loss mechanisms on two different linear spectra, absorption spectra and CD spectra, of condensed phase systems using the recently developed PILD method. Empirical loss mechanisms are often incorporated using non-Hermitian descriptions, which make the time-evolution nonunitary. This has spurious effects on the spectra. PILD ensures that the dynamical maps are unitary and, consequently, avoids such spurious effects. An additional benefit of PILD is that one can get the effect of these loss mechanisms at no extra cost while maintaining the accuracy of the method and the rigor of accounting for the effects of the thermal dissipative environment. One of the consequences of the accuracy of these simulations is that the area under the spectra is invariant with the changing timescale of the losses.

https://doi.org/10.1021/acs.jctc.4c00825
J. Chem. Theory Comput. XXXX, XXX, XXX−XXX

Table 2. Absorption and CD Peak Heights for Isolated Polaritonic Aggregates as a Function of Aggregate Size[a]

polaritonic aggregate	helix			creeper		
	ω' (cm^{-1})	$\sigma_{CD}(\omega')$	$\sigma_{abs}(\omega')$	ω' (cm^{-1})	$\sigma_{CD}(\omega')$	$\sigma_{abs}(\omega')$
dimer	−367.21	+0.48	0.14	−599.47	−0.36	1.32
	−232.26	−0.12	0.52	+232.26	−0.12	0.52
	+599.47	−0.36	1.32	+367.21	+0.48	0.14
trimer	−515.89	−0.20	0.04	−666.80	−1.28	2.00
	−179.78	+0.08	0.42	−28.88	+1.41	0.53
	+28.88	+1.41	0.53	+179.78	+0.08	0.42
	+666.80	−1.28	2.00	+515.89	−0.20	0.04

[a] $\omega' = \omega - \varepsilon$.

Intuitively, one might think that the effect of loss is a broadening of the spectrum. This is indeed the primary effect. However, the details are much more complex. Different peaks get broadened by different amounts based on where the loss is present. The presence of the environment that couples to the system has the potential to change the impact of the empirical loss on the spectra as well. Additionally, this excess broadening is also accompanied by a shift of the peaks. Our current work provides a rigorous framework allowing simulations to quantitatively predict the spectra of condensed phase systems in the presence of empirical loss.

We consider the absorption and CD spectra of chiral excitonic aggregates and chiral polaritonic aggregates formed by these systems inside a nonchiral, plane-polarized cavity. The numerically exact spectra of the excitonic aggregates are already quite complicated. We show that different peaks are attenuated at different rates. The contribution of a state, which stages the loss, to an exciton, while an important consideration, is not the only factor that determines the amount by which the relevant peak would get attenuated. The vibronic couplings due to the thermal environment couple different excitons together, leading to a rather convoluted impact of the loss on various peaks. We also consider the effect of loss on aggregates of different sizes. Because the loss considered here is localized on a single site, for the same decay time constant τ, the impact is the highest on the small aggregates. The relative attenuation decreases with growing size of the aggregates. It should, however, be noted that while not explored here, PILD is capable of dealing with multiple loss sites simultaneously.

The presence of the cavity adds to the complexity of the problem. The excitonic absorption peaks split into multiple polaritonic peaks. We report probably the first numerically exact path integral simulations of CD spectra of chiral aggregates in a cavity. The chirality of the different polaritonic peaks interacts in unexpected manners. For a monomer or a dimer, for instance, the upper polariton is attenuated significantly less than the lower polariton.

We also demonstrate that the behavior of lossy excitonic and polaritonic aggregates in the presence and absence of dissipative environments differ in a qualitative fashion. In the absence of the dissipative medium, the peaks broaden and come closer to each other on decreasing the loss decay constant. In the context of polaritonic cavities, this is exactly what is known from the so-called coupled-oscillator theory using non-Hermitian descriptions of the system.[58] This is irrespective of the relative magnitudes of the lossy decay and the intersite couplings. However, this observation changes when the dissipative environment is brought into the picture. According to $P(E)$ theory,[58,59] for the cases of strong intersite coupling relative to the decay, peaks broaden and move apart. In the weak coupling regime, they broaden and come together, similar to the case of the isolated system. Through our simulations of numerically exact spectra of chiral aggregates, we have demonstrated that though we do not have a single intersite coupling to provide a scale, the emergent effect of the complex interactions leads to a phenomenon that is close to the case of the strong coupling limit as described by $P(E)$ theory.[58]

While some of these effects are intuitive, many others are not. Additionally, the magnitude of a particular effect cannot be predicted without simulations of specific systems under the exact conditions. This necessitates rigorous simulation frameworks for predicting the spectra in these open quantum systems. In this work, we demonstrated the effectiveness of PILD in providing the exact spectra in the presence of loss incorporating the dissipative environment in a nonperturbative manner using the path integral calculations. While the current work is primarily about the simulation method, we hope that the surprising differences between the impact of the cavity and molecular loss on spectra will serve to motivate further experimental explorations of similar ideas. The ability to understand and predict the spectra provides a powerful handle on the properties of these complex aggregates. This would be a topic of exploration and study in the future, where PILD will provide the basis for the exploration of multidimensional spectra and how loss changes them. Furthermore, equally interesting is the prospect of understanding transport in complex systems with losses, and these numerically exact methods promise to be exceptionally useful in understanding such transports, the routes involved, and relative efficiencies. These facets will be developed in the near future.

APPENDIX A

Spectra of Lossy Systems without Vibrational Decohering Environments

To understand the changes better, we demonstrate the impact of the loss analytically on the spectra of a planar excitonic dimer and a monomer interacting with a cavity mode without any thermal environment. This can be done analytically and enables separation of impact caused solely by the loss versus that caused through the mediation of the environment.

Consider first the excitonic dimer without the dissipative environment as defined in eq 2 with equal monomer excitation energy ε and intermonomer coupling as $h_{12}(=h_{21})$. As in the cases described earlier, there is a loss with a time-scale of τ on the second monomer given by $L_2 = \tau^{-1/2}|0\rangle\langle 2|$. For simplicity of analysis, we assume that the decay time scale is relatively weak, $\tau > \frac{\hbar}{4|h_{12}|}$. This would typically be the case because the electronic couplings between the monomers would be stronger

https://doi.org/10.1021/acs.jctc.4c00825
J. Chem. Theory Comput. XXXX, XXX, XXX−XXX

than the time-scales of a loss process. The transition dipole moment operator is defined in eq 18 with equal magnitudes μ for each monomer.

The absorption spectrum can now be calculated using the relation 15 to get

$$\sigma_{\mathrm{abs}}^{(2)}(\omega) \propto \mu^2 \frac{b}{a}\left[\frac{a + h_{12}/\hbar}{(\omega - a - \varepsilon/\hbar)^2 + b^2} + \frac{a - h_{12}/\hbar}{(\omega + a - \varepsilon/\hbar)^2 + b^2}\right] \tag{19}$$

where $a = \sqrt{\frac{h_{12}^2}{\hbar^2} - \frac{1}{16\tau^2}}$ and $b = \frac{1}{4\tau}$. Notice that this is a sum of two Lorentzians centered at $\omega_+ = \varepsilon/\hbar + a$ and $\omega_- = \varepsilon/\hbar - a$, respectively. For $\tau \gg \frac{\hbar}{4h_{12}}$, $a = \frac{|h_{12}|}{\hbar} - \frac{1}{32}\frac{\hbar}{\tau^2 h_{12}}$. If $h_{12} > 0$ (H-type dimer), the intensity of the peak at ω_- would be very small and can be neglected. Consequently, on decreasing τ (i.e., a stronger decay), the dominant peak at ω_+ shows a red shift owing to the decrease in the value of a. A similar analysis shows that when $h_{12} < 0$ (J-type dimer), the peak at ω_+ would have a negligible height, and the peak at ω_- shows a blue shift. Notice that having a loss gives rise to a nonzero amplitude of the other peak as well. The peak at ω_- (ω_+) would be typically symmetry forbidden for an H-dimer (J-dimer). However, here we see these peaks gaining small nonzero intensities. For $\tau < \frac{\hbar}{4|h_{12}|}$, both the peaks merge into one at $\varepsilon/\hbar$. This result is similar to what one observes using non-Hermitian descriptions of loss in the so-called coupled-oscillator model.[58]

Similarly, for a monomer-cavity system defined with eq 17 for a cavity resonant with monomer excitation energy, $\hbar\omega_c = \varepsilon$, monomer-cavity coupling Ω, and transition dipole moment as defined in eq 18 with magnitude μ, we consider two cases with a loss on the cavity $L_c = \tau^{-1/2}|0\rangle\langle c|$ and a loss on the monomer $L_1 = \tau^{-1/2}|0\rangle\langle 1|$. The corresponding absorption spectra for the loss on the cavity and the monomer are

$$\sigma_{\mathrm{abs}}^{(c)}(\omega) \propto \mu^2 \frac{b}{2a'}\left[\frac{2a' - \omega + \varepsilon/\hbar}{(\omega - a' - \varepsilon/\hbar)^2 + b^2} + \frac{2a' + \omega - \varepsilon/\hbar}{(\omega + a' - \varepsilon/\hbar)^2 + b^2}\right] \tag{20}$$

$$\sigma_{\mathrm{abs}}^{(1)}(\omega) \propto \mu^2 \frac{b}{2a'}\left[\frac{\omega - \varepsilon/\hbar}{(\omega - a' - \varepsilon/\hbar)^2 + b^2} - \frac{\omega - \varepsilon/\hbar}{(\omega + a' - \varepsilon/\hbar)^2 + b^2}\right] \tag{21}$$

Here, $a' = \sqrt{\frac{\Omega^2}{\hbar^2} - \frac{1}{16\tau^2}}$, which is the same as a but with h_{12} replaced by Ω, while the symbol in superscript parentheses denotes the site of loss.

We can now see from relation 20 that for the loss on cavity, instead of shifting in the same direction, the lower-energy polariton shifts to blue, whereas the higher-energy polariton shifts to red. This is exactly opposite to what we saw in the presence of the dissipative media (Figure 5). However, with relation 21 for the loss on monomer, there is no conspicuous shift in the spectrum. It is also to be noted that the line shape for the two polaritonic peaks are symmetrical despite the inclusion of loss at any site.

APPENDIX B

Rotatory Strengths for Peaks of Excitonic and Polaritonic Aggregates

Here, we discuss the rotatory strength matrix for bare excitonic and polaritonic aggregates in the absence of thermal dissipative environments. Consider a general aggregate, either excitonic or polaritonic, described by a Hamiltonian $\widehat{H}_0$ with N molecules located at $\vec{\mathbf{r}}_j$ with transition dipoles $\vec{\mu}_j$. The cross-correlation function between the transition dipole moment and the magnetic moment can be refactored as follows[48,57]

$$\sigma_{\mathrm{CD}}(\omega) \propto \mathrm{Re}\int_0^\infty \mathrm{d}t \sum_{ij} R_{ji} I_{ij}(t)\exp(i\omega t) \tag{22}$$

where

$$R_{ji} = -\sqrt{\varepsilon_i \varepsilon_j}(\vec{\mathbf{r}}_j - \vec{\mathbf{r}}_i)\cdot(\vec{\mu}_i \times \vec{\mu}_j) \tag{23}$$

$$I_{ij}(t) = \frac{1}{2\hbar} e^{iE_g t/\hbar}\mathrm{Tr}_{\mathrm{env}}(\langle j|e^{-iHt/\hbar}|i\rangle) \tag{24}$$

where H is the total Hamiltonian including the environment. The rotatory strength matrix is R and $I(t)$ is the line shape function. Now, this is defined in the molecular basis. We want the strengths corresponding to the different eigenstates of the system Hamiltonian $\widehat{H}_0$, $|e_j\rangle$. These states, $|e_j\rangle$, correspond to excitons in the molecular aggregates and polaritons in the presence of cavities. It is possible to transform the spectrum from a molecular basis to the eigenstate basis

$$\sigma_{\mathrm{CD}}(\omega) \propto \mathrm{Re}\int_0^\infty \mathrm{d}t\ \mathrm{Tr}(RI(t))\exp(i\omega t) \tag{25}$$

$$\propto \mathrm{Re}\int_0^\infty \mathrm{d}t \sum_{ij} \langle e_i|R|e_j\rangle\langle e_j|I(t)|e_i\rangle\exp(i\omega t) \tag{26}$$

For an isolated system in the absence of a dissipative environment, the transformation is simple. The line shape function matrix $I(t)$ is diagonal in the $|e_j\rangle$ basis. It is the presence of the dissipative environment that couples the different eigenstates. Consequently, the peak heights for an isolated system are proportional to the matrix element of the rotatory strength matrix corresponding to the particular eigenstate, $\langle e_j|R|e_j\rangle$.

$$\sigma_{\mathrm{CD}}(\omega) \propto \sum_i \langle e_i|R|e_i\rangle\delta(\omega - E_i/\hbar + E_g/\hbar) \tag{27}$$

APPENDIX C

Absorption and CD Peak Heights for Isolated Excitonic and Polaritonic Aggregates

Here, we present the absorption and CD peak positions and their heights for the excitonic and polaritonic systems discussed in Section 3 in the absence of a thermal environment.

Notice in the following Tables 1 and 2 that in the absence of the thermal environment, the absorption and CD peak heights are exactly reversed (modulo a proportionality constant) between the helix and the creeper. In particular, for the excitonic aggregates, the peak positions of the creeper and helix

https://doi.org/10.1021/acs.jctc.4c00825
J. Chem. Theory Comput. XXXX, XXX, XXX−XXX

coincide albeit with reversed peak heights. The excitonic creeper always has a negative first peak and a positive second peak in the CD spectrum, which grow more intense with the size of the aggregate, as also seen in the presence of a thermal environment. However, there is no apparent pattern for the excitonic helix with regard to the sign of the first CD peak. We see that the sign of the first peak of the helix keeps alternating between a positive and a negative sign. This apparently simple pattern for helices is further complicated by the fact that some times, like in the case of an excitonic pentamer, the first CD peak has zero intensity. In that case, effectively, the first peak that is symmetry allowed would be positive again. For the polaritonic aggregates, we see more than two bright polaritonic states in the absorption spectra as noted and discussed in Section 3.2. The polaritonic creepers' first CD couplet, unlike in the excitonic case, shows no regular pattern. All these patterns are consistent with the spectra calculated in the presence of the solvent.

AUTHOR INFORMATION

Corresponding Author

Amartya Bose − *Department of Chemical Sciences, Tata Institute of Fundamental Research, Mumbai 400005, India;* orcid.org/0000-0003-0685-5096; Email: amartya.bose@tifr.res.in

Author

Devansh Sharma − *Department of Chemical Sciences, Tata Institute of Fundamental Research, Mumbai 400005, India*

Complete contact information is available at: https://pubs.acs.org/10.1021/acs.jctc.4c00825

Notes

The authors declare no competing financial interest.

REFERENCES

(1) White, S. R. Density Matrix Formulation for Quantum Renormalization Groups. *Phys. Rev. Lett.* **1992**, *69*, 2863−2866.
(2) Schollwöck, U. The Density-Matrix Renormalization Group. *Rev. Mod. Phys.* **2005**, *77*, 259−315.
(3) Schollwöck, U. The Density-Matrix Renormalization Group in the Age of Matrix Product States. *Ann. Phys.* **2011**, *326*, 96−192.
(4) Paeckel, S.; Köhler, T.; Swoboda, A.; Manmana, S. R.; Schollwöck, U.; Hubig, C. Time-Evolution Methods for Matrix-Product States. *Ann. Phys.* **2019**, *411*, 167998.
(5) Meyer, H.-D.; Manthe, U.; Cederbaum, L. The Multi-Configurational Time-Dependent Hartree Approach. *Chem. Phys. Lett.* **1990**, *165*, 73−78.
(6) Wang, H.; Thoss, M. Multilayer Formulation of the Multi-configuration Time-Dependent Hartree Theory. *J. Chem. Phys.* **2003**, *119*, 1289−1299.
(7) Wang, H. Multilayer Multiconfiguration Time-Dependent Hartree Theory. *J. Phys. Chem. A* **2015**, *119*, 7951−7965.
(8) Bloch, F. Generalized Theory of Relaxation. *Phys. Rev.* **1957**, *105*, 1206−1222.
(9) Redfield, A. G. On the Theory of Relaxation Processes. *IBM J. Res. Dev.* **1957**, *1*, 19−31.
(10) Lindblad, G. On the Generators of Quantum Dynamical Semigroups. *Commun. Math. Phys.* **1976**, *48*, 119−130.
(11) Gorini, V.; Kossakowski, A.; Sudarshan, E. C. G. Completely Positive Dynamical Semigroups of N-level Systems. *J. Math. Phys.* **1976**, *17*, 821−825.
(12) Tully, J. C. Molecular Dynamics with Electronic Transitions. *J. Chem. Phys.* **1990**, *93*, 1061−1071.
(13) Tully, J. C.; Preston, R. K. Trajectory Surface Hopping Approach to Nonadiabatic Molecular Collisions: The Reaction of H+ with D2. *J. Chem. Phys.* **1971**, *55*, 562−572.
(14) Feynman, R. P.; Hibbs, A. R.; Styer, D. F. *Quantum Mechanics and Path Integrals*. emended ed.; Dover Publications: Mineola, N.Y, 2010.
(15) Feynman, R. P.; Vernon, F. L. The Theory of a General Quantum System Interacting with a Linear Dissipative System. *Ann. Phys.* **1963**, *24*, 118−173.
(16) Tanimura, Y.; Wolynes, P. G. Quantum and Classical Fokker-Planck Equations for a Gaussian-Markovian Noise Bath. *Phys. Rev. A* **1991**, *43*, 4131−4142.
(17) Tanimura, Y. Numerically "Exact" Approach to Open Quantum Dynamics: The Hierarchical Equations of Motion (HEOM). *J. Chem. Phys.* **2020**, *153*, 20901.
(18) Makri, N.; Makarov, D. E. Tensor Propagator for Iterative Quantum Time Evolution of Reduced Density Matrices. I. Theory. *J. Chem. Phys.* **1995**, *102*, 4600−4610.
(19) Makri, N.; Makarov, D. E. Tensor Propagator for Iterative Quantum Time Evolution of Reduced Density Matrices. II. Numerical Methodology. *J. Chem. Phys.* **1995**, *102*, 4611−4618.
(20) Cerrillo, J.; Cao, J. Non-Markovian Dynamical Maps: Numerical Processing of Open Quantum Trajectories. *Phys. Rev. Lett.* **2014**, *112*, 110401.
(21) Rahman, H.; Kleinekathöfer, U. Chebyshev Hierarchical Equations of Motion for Systems with Arbitrary Spectral Densities and Temperatures. *J. Chem. Phys.* **2019**, *150*, 244104.
(22) Xu, M.; Yan, Y.; Shi, Q.; Ankerhold, J.; Stockburger, J. T. Taming Quantum Noise for Efficient Low Temperature Simulations of Open Quantum Systems. *Phys. Rev. Lett.* **2022**, *129*, 230601.
(23) Strathearn, A.; Kirton, P.; Kilda, D.; Keeling, J.; Lovett, B. W. Efficient Non-Markovian Quantum Dynamics Using Time-Evolving Matrix Product Operators. *Nat. Commun.* **2018**, *9*, 3322.
(24) Jørgensen, M. R.; Pollock, F. A. Exploiting the Causal Tensor Network Structure of Quantum Processes to Efficiently Simulate Non-Markovian Path Integrals. *Phys. Rev. Lett.* **2019**, *123*, 240602.
(25) Makri, N. Small Matrix Disentanglement of the Path Integral: Overcoming the Exponential Tensor Scaling with Memory Length. *J. Chem. Phys.* **2020**, *152*, 41104.
(26) Bose, A.; Walters, P. L. A Multisite Decomposition of the Tensor Network Path Integrals. *J. Chem. Phys.* **2022**, *156*, 024101.
(27) Bose, A.; Walters, P. L. Impact of Solvent on State-to-State Population Transport in Multistate Systems Using Coherences. *J. Chem. Theory Comput.* **2023**, *19*, 4828−4836.
(28) Bose, A. Quantum Correlation Functions through Tensor Network Path Integral. *J. Chem. Phys.* **2023**, *159*, 214110.
(29) Yan, Y.; Xu, M.; Li, T.; Shi, Q. Efficient Propagation of the Hierarchical Equations of Motion Using the Tucker and Hierarchical Tucker Tensors. *J. Chem. Phys.* **2021**, *154*, 194104.
(30) Kundu, S.; Dani, R.; Makri, N. B800-to-B850 Relaxation of Excitation Energy in Bacterial Light Harvesting: All-state, All-Mode Path Integral Simulations. *J. Chem. Phys.* **2022**, *157*, 015101.
(31) Bose, A.; Walters, P. L. Tensor Network Path Integral Study of Dynamics in B850 LH2 Ring with Atomistically Derived Vibrations. *J. Chem. Theory Comput.* **2022**, *18*, 4095−4108.
(32) Bose, A.; Walters, P. L. Impact of Spatial Inhomogeneity on Excitation Energy Transport in the Fenna−Matthews−Olson Complex. *J. Phys. Chem. B* **2023**, *127*, 7663−7673.
(33) Bose, A.; Walters, P. L. A Tensor Network Representation of Path Integrals: Implementation and Analysis. *arXiv* **2021**, arXiv:2106.12523.
(34) Gardiner, C. W.; Collett, M. J. Input and output in damped quantum systems: Quantum stochastic differential equations and the master equation. *Phys. Rev. A* **1985**, *31*, 3761−3774.
(35) Bose, A. Pairwise Connected Tensor Network Representation of Path Integrals. *Phys. Rev. B* **2022**, *105*, 024309.
(36) Huo, P.; Coker, D. F. Communication: Partial Linearized Density Matrix Dynamics for Dissipative, Non-Adiabatic Quantum Evolution. *J. Chem. Phys.* **2011**, *135*, 201101.

(37) Provazza, J.; Segatta, F.; Garavelli, M.; Coker, D. F. Semiclassical Path Integral Calculation of Nonlinear Optical Spectroscopy. *J. Chem. Theory Comput.* **2018**, *14*, 856−866.
(38) Mondal, M. E.; Koessler, E. R.; Provazza, J.; Vamivakas, A. N.; Cundiff, S. T.; Krauss, T. D.; Huo, P. Quantum Dynamics Simulations of the 2D Spectroscopy for Exciton Polaritons. *J. Chem. Phys.* **2023**, *159*, 094102.
(39) Bose, A. Incorporation of Empirical Gain and Loss Mechanisms in Open Quantum Systems through Path Integral Lindblad Dynamics. *J. Phys. Chem. Lett.* **2024**, *15*, 3363−3368.
(40) Olbrich, C.; Strümpfer, J.; Schulten, K.; Kleinekathöfer, U. Theory and Simulation of the Environmental Effects on FMO Electronic Transitions. *J. Phys. Chem. Lett.* **2011**, *2*, 1771−1776.
(41) Maity, S.; Bold, B. M.; Prajapati, J. D.; Sokolov, M.; Kubař, T.; Elstner, M.; Kleinekathöfer, U. DFTB/MM Molecular Dynamics Simulations of the FMO Light-Harvesting Complex. *J. Phys. Chem. Lett.* **2020**, *11*, 8660−8667.
(42) Bose, A. Zero-Cost Corrections to Influence Functional Coefficients from Bath Response Functions. *J. Chem. Phys.* **2022**, *157*, 054107.
(43) Nakajima, S. On Quantum Theory of Transport Phenomena. *Prog. Theor. Phys.* **1958**, *20*, 948−959.
(44) Zwanzig, R. Ensemble Method in the Theory of Irreversibility. *J. Chem. Phys.* **1960**, *33*, 1338−1341.
(45) Mulvihill, E.; Schubert, A.; Sun, X.; Dunietz, B. D.; Geva, E. A Modified Approach for Simulating Electronically Nonadiabatic Dynamics via the Generalized Quantum Master Equation. *J. Chem. Phys.* **2019**, *150*, 034101.
(46) Mulvihill, E.; Geva, E. A Road Map to Various Pathways for Calculating the Memory Kernel of the Generalized Quantum Master Equation. *J. Phys. Chem. B* **2021**, *125*, 9834−9852.
(47) Buser, M.; Cerrillo, J.; Schaller, G.; Cao, J. Initial System-Environment Correlations via the Transfer-Tensor Method. *Phys. Rev. A: At., Mol., Opt. Phys.* **2017**, *96*, 062122.
(48) Dinh, T.-C.; Renger, T. Towards an exact theory of linear absorbance and circular dichroism of pigment-protein complexes: Importance of non-secular contributions. *J. Chem. Phys.* **2015**, *142*, 034104.
(49) Tretiak, S.; Middleton, C.; Chernyak, V.; Mukamel, S. Bacteriochlorophyll and Carotenoid Excitonic Couplings in the LH2 System of Purple Bacteria. *J. Phys. Chem. B* **2000**, *104*, 9540−9553.
(50) Rätsep, M.; Cai, Z.-L.; Reimers, J. R.; Freiberg, A. Demonstration and Interpretation of Significant Asymmetry in the Low-Resolution and High-Resolution Qy Fluorescence and Absorption Spectra of Bacteriochlorophyll a. *J. Chem. Phys.* **2011**, *134*, 24506.
(51) Bose, A. QuantumDynamics.Jl: A Modular Approach to Simulations of Dynamics of Open Quantum Systems. *J. Chem. Phys.* **2023**, *158*, 204113.
(52) Hestand, N. J.; Spano, F. C. Expanded Theory of H- and J-Molecular Aggregates: The Effects of Vibronic Coupling and Intermolecular Charge Transfer. *Chem. Rev.* **2018**, *118*, 7069−7163.
(53) Harada, N.; Chen, S.-M. L.; Nakanishi, K. Quantitative definition of exciton chirality and the distant effect in the exciton chirality method. *J. Am. Chem. Soc.* **1975**, *97*, 5345−5352.
(54) Harada, N.; Nakanishi, K.; Berova, N. *Comprehensive Chiroptical Spectroscopy*; John Wiley & Sons, Ltd, 2012; Chapter 4, pp 115−166.
(55) Harada, N.; Nakanishi, K. Optical rotatory power of the benzoate group. *J. Am. Chem. Soc.* **1968**, *90*, 7351−7352.
(56) Swathi, K.; Sissa, C.; Painelli, A.; George Thomas, K. Supramolecular chirality: a caveat in assigning the handedness of chiral aggregates. *Chem. Commun.* **2020**, *56*, 8281−8284.
(57) Cupellini, L.; Lipparini, F.; Cao, J. Absorption and Circular Dichroism Spectra of Molecular Aggregates With the Full Cumulant Expansion. *J. Phys. Chem. B* **2020**, *124*, 8610−8617.
(58) Kansanen, K. S. U.; Toppari, J. J.; Heikkilä, T. T. Polariton Response in the Presence of Brownian Dissipation from Molecular Vibrations. *J. Chem. Phys.* **2021**, *154*, 044108.
(59) Kansanen, K. S. U.; Asikainen, A.; Toppari, J. J.; Groenhof, G.; Heikkilä, T. T. Theory for the Stationary Polariton Response in the Presence of Vibrations. *Phys. Rev. B* **2019**, *100*, 245426.
(60) Herrera, F.; Spano, F. C. Cavity-Controlled Chemistry in Molecular Ensembles. *Phys. Rev. Lett.* **2016**, *116*, 238301.

https://doi.org/10.1021/acs.jctc.4c00825
J. Chem. Theory Comput. XXXX, XXX, XXX−XXX